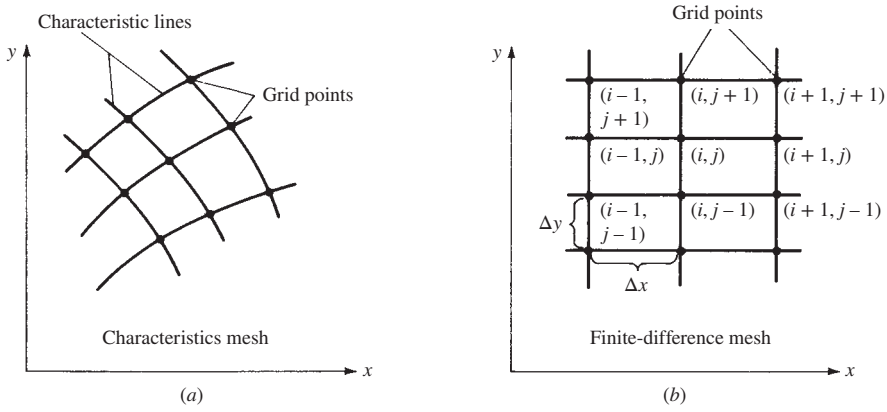

Figure 13.2 Grid points.

techniques, although others may prefer to list it under a more classical heading. We also show how the method of characteristics is applied to design the divergent contour of a supersonic nozzle. Then we move to a discussion of the finite-difference approach, which we will use to illustrate the application of CFD to nozzle flows and the flow over a supersonic blunt body.

In contrast to the linearized solutions discussed in Chapters 11 and 12, CFD represents numerical solutions to the *exact* nonlinear governing equations, that is, the equations without simplifying assumptions such as small perturbations, and which apply to all speed regimes, transonic and hypersonic as well as subsonic and supersonic. Although numerical roundoff and truncation errors are always present in any numerical representation of the governing equations, we still think of CFD solutions as being "exact solutions."

Both the method of characteristics and finite-difference methods have one thing in common: They represent a continuous flow field by a series of distinct grid points in space, as shown in Figure 13.2. The flow-field properties (u, v, p, T, etc.) are calculated at each one of these grid points. The mesh generated by these grid points is generally skewed for the method of characteristics, as shown in Figure 13.2*a*, but is usually rectangular for finite-difference solutions, as shown in Figure 13.2*b*. We will soon appreciate why these different meshes occur.

13.2 ELEMENTS OF THE METHOD OF CHARACTERISTICS

In this section, we only introduce the basic elements of the method of characteristics. A full discussion is beyond the scope of this book; see References 21, 25, and 32 for more details.

Consider a two-dimensional, steady, inviscid, supersonic flow in xy space, as given in Figure 13.2*a*. The flow variables (p, u, T, etc.) are continuous throughout

this space. However, there are certain lines in xy space along which the *derivatives* of the flow field variables ($\partial p/\partial x$, $\partial u/\partial y$, etc.) are *indeterminate* and across which may even be discontinuous. Such lines are called *characteristic lines*. This may sound strange at first; however, let us prove that such lines exist, and let us find their precise directions in the xy plane.

In addition to the flow being supersonic, steady, inviscid, and two-dimensional, assume that it is also irrotational. The exact governing equation for such a flow is given by Equation (11.12):

$$\left[1 - \frac{1}{a^2}\left(\frac{\partial \phi}{\partial x}\right)^2\right]\frac{\partial^2 \phi}{\partial x^2} + \left[1 - \frac{1}{a^2}\left(\frac{\partial \phi}{\partial y}\right)^2\right]\frac{\partial^2 \phi}{\partial y^2} - \frac{2}{a^2}\frac{\partial \phi}{\partial x}\frac{\partial \phi}{\partial y}\frac{\partial^2 \phi}{\partial x\,\partial y} = 0 \tag{11.12}$$

[Keep in mind that we are dealing with the full velocity potential ϕ in Equation (11.12), not the perturbation potential.] Since $\partial \phi/\partial x = u$ and $\partial \phi/\partial y = v$, Equation (11.12) can be written as

$$\left(1 - \frac{u^2}{a^2}\right)\frac{\partial^2 \phi}{\partial x^2} + \left(1 - \frac{v^2}{a^2}\right)\frac{\partial^2 \phi}{\partial y^2} - \frac{2uv}{a^2}\frac{\partial^2 \phi}{\partial x\,\partial y} = 0 \tag{13.1}$$

The velocity potential and its derivatives are functions of x and y, for example,

$$\frac{\partial \phi}{\partial x} = f(x, y)$$

Hence, from the relation for an exact differential,

$$df = \frac{\partial f}{\partial x}dx + \frac{\partial f}{\partial y}dy$$

we have

$$d\left(\frac{\partial \phi}{\partial x}\right) = du = \frac{\partial^2 \phi}{\partial x^2}dx + \frac{\partial^2 \phi}{\partial x\,\partial y}dy \tag{13.2}$$

Similarly,

$$d\left(\frac{\partial \phi}{\partial y}\right) = dv = \frac{\partial^2 \phi}{\partial x\,\partial y}dx + \frac{\partial^2 \phi}{\partial y^2}dy \tag{13.3}$$

Examine Equations (13.1) to (13.3) closely. Note that they contain the second derivatives $\partial^2 \phi/\partial x^2$, $\partial^2 \phi/\partial y^2$, and $\partial^2 \phi/\partial x\,\partial y$. If we imagine these derivatives as "unknowns," then Equations (13.1), (13.2), and (13.3) represent three equations with three unknowns. For example, to solve for $\partial^2 \phi/\partial x\,\partial y$, use Cramer's rule as follows:

$$\frac{\partial^2 \phi}{\partial x\,\partial y} = \frac{\begin{vmatrix} 1 - \dfrac{u^2}{a^2} & 0 & 1 - \dfrac{v^2}{a^2} \\ dx & du & 0 \\ 0 & dv & dy \end{vmatrix}}{\begin{vmatrix} 1 - \dfrac{u^2}{a^2} & -\dfrac{2uv}{a^2} & 1 - \dfrac{v^2}{a^2} \\ dx & dy & 0 \\ 0 & dx & dy \end{vmatrix}} = \frac{N}{D} \tag{13.4}$$

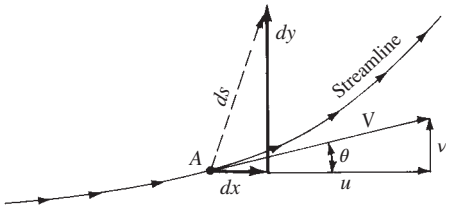

Figure 13.3 An arbitrary direction *ds* away from point *A*.

where N and D represent the numerator and denominator determinants, respectively. The physical meaning of Equation (13.4) can be seen by considering point A and its surrounding neighborhood in the flow, as sketched in Figure 13.3. The derivative $\partial^2\phi/\partial x\,\partial y$ has a specific value at point A. Equation (13.4) gives the solution for $\partial^2\phi/\partial x\,\partial y$ for an *arbitrary* choice of dx and dy. The combination of dx and dy defines an arbitrary direction ds away from point A as shown in Figure 13.3. In general, this direction is different from the streamline direction going through point A. In Equation (13.4), the differentials du and dv represent the changes in velocity that take place over the increments dx and dy. Hence, although the choice of dx and dy is arbitrary, the values of du and dv in Equation (13.4) must correspond to this choice. No matter what values of dx and dy are arbitrarily chosen, the corresponding values of du and dv will always ensure obtaining the same value of $\partial^2\phi/\partial x\,\partial y$ at point A from Equation (13.4).

The single exception to the above comments occurs when dx and dy are chosen so that $D = 0$ in Equation (13.4). In this case, $\partial^2\phi/\partial x\,\partial y$ is not defined. This situation will occur for a specific direction ds away from point A in Figure 13.3, defined for that specific combination of dx and dy for which $D = 0$. However, we know that $\partial^2\phi/\partial x\,\partial y$ has a specific defined value at point A. Therefore, the only consistent result associated with $D = 0$ is that $N = 0$, also; that is,

$$\frac{\partial^2\phi}{\partial x\,\partial y} = \frac{N}{D} = \frac{0}{0} \tag{13.5}$$

Here, $\partial^2\phi/\partial x\,\partial y$ is an indeterminate form, which is allowed to be a finite value, that is, that value of $\partial^2\phi/\partial x\,\partial y$ which we know exists at point A. *The important conclusion here is that there is some direction (or directions) through point A along which* $\partial^2\phi/\partial x\,\partial y$ *is indeterminate.* Since $\partial^2\phi/\partial x\,\partial y = \partial u/\partial y = \partial v/\partial x$, this implies that the derivatives of the flow variables are indeterminate along these lines. Hence, we have proven that lines do exist in the flow field along which derivatives of the flow variables are indeterminate; earlier, we defined such lines as *characteristic lines*.

Consider again point A in Figure 13.3. From our previous discussion, there are one or more characteristic lines through point A. *Question:* How can we calculate the precise direction of these characteristic lines? The answer can be obtained by setting $D = 0$ in Equation (13.4). Expanding the denominator determinant in

Equation (13.4), and setting it equal to zero, we have

$$\left(1-\frac{u^2}{a^2}\right)(dy)^2+\frac{2uv}{a^2}dx\,dy+\left(1-\frac{v^2}{a^2}\right)(dx)^2=0$$

or

$$\left(1-\frac{u^2}{a^2}\right)\left(\frac{dy}{dx}\right)_{\text{char}}^2+\frac{2uv}{a^2}\left(\frac{dy}{dx}\right)_{\text{char}}+\left(1-\frac{v^2}{a^2}\right)=0 \tag{13.6}$$

In Equation (13.6), dy/dx is the slope of the characteristic lines; hence, the subscript "char" has been added to emphasize this fact. Solving Equation (13.6) for $(dy/dx)_{\text{char}}$ by means of the quadratic formula, we obtain

$$\left(\frac{dy}{dx}\right)_{\text{char}}=\frac{-2uv/a^2\pm\sqrt{(2uv/a^2)^2-4(1-u^2/a^2)(1-v^2/a^2)}}{2(1-u^2/a^2)}$$

or

$$\left(\frac{dy}{dx}\right)_{\text{char}}=\frac{-uv/a^2\pm\sqrt{(u^2+v^2)/a^2-1}}{1-u^2/a^2} \tag{13.7}$$

From Figure 13.3, we see that $u = V\cos\theta$ and $v = V\sin\theta$. Hence, Equation (13.7) becomes

$$\left(\frac{dy}{dx}\right)_{\text{char}}=\frac{(-V^2\cos\theta\sin\theta)/a^2\pm\sqrt{(V^2/a^2)(\cos^2\theta+\sin^2\theta)-1}}{1-[(V^2/a^2)\cos^2\theta]} \tag{13.8}$$

Recall that the local Mach angle μ is given by $\mu=\sin^{-1}(1/M)$, or $\sin\mu=1/M$. Thus, $V^2/a^2=M^2=1/\sin^2\mu$, and Equation (13.8) becomes

$$\left(\frac{dy}{dx}\right)_{\text{char}}=\frac{(-\cos\theta\sin\theta)/\sin^2\mu\pm\sqrt{(\cos^2\theta+\sin^2\theta)/\sin^2\mu-1}}{1-(\cos^2\theta)/\sin^2\mu} \tag{13.9}$$

After considerable algebraic and trigonometric manipulation, Equation (13.9) reduces to

$$\boxed{\left(\frac{dy}{dx}\right)_{\text{char}}=\tan(\theta\mp\mu)} \tag{13.10}$$

Equation (13.10) is an important result; it states that *two* characteristic lines run through point A in Figure 13.3, namely, one line with a slope equal to $\tan(\theta-\mu)$ and the other with a slope equal to $\tan(\theta+\mu)$. The physical significance of this result is illustrated in Figure 13.4. Here, a streamline through point A is inclined at the angle θ with respect to the horizontal. The velocity at point A is V, which also makes the angle θ with respect to the horizontal. Equation (13.10) states that one characteristic line at point A is inclined *below* the streamline direction by the angle μ; this characteristic line is labeled as C_- in Figure 13.4. Equation (13.10) also states that the other characteristic line at point A is inclined *above* the streamline direction by the angle μ; this characteristic line is labeled as C_+ in Figure 13.4. Examining Figure 13.4, we see that the characteristic lines through

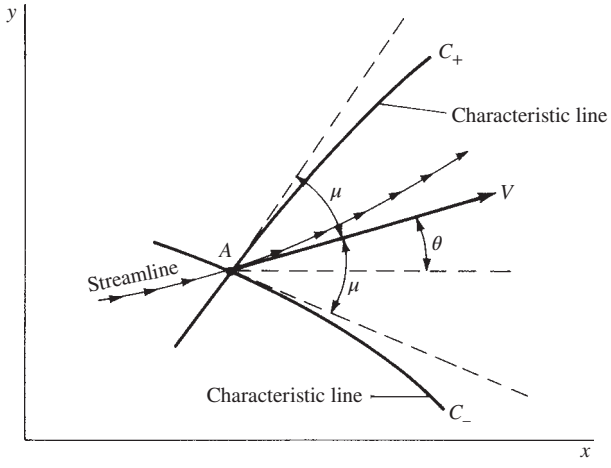

Figure 13.4 Left- and right-running characteristic lines through point *A*.

point *A* are simply the left- and right-running *Mach waves* through point *A*. Hence, *the characteristic lines are Mach lines*. In Figure 13.4, the left-running Mach wave is denoted by C_+, and the right-running Mach wave is denoted by C_-. Hence, returning to Figure 13.2*a*, the characteristics mesh consists of left- and right-running Mach waves that crisscross the flow field. There are an infinite number of these waves; however, for practical calculations we deal with a finite number of waves, the intersections of which define the grid points shown in Figure 13.2*a*. Note that the characteristic lines are curved in space because (1) the local Mach angle depends on the local Mach number, which is a function of x and y, and (2) the local streamline direction θ varies throughout the flow.

The characteristic lines in Figure 13.2*a* are of no use to us by themselves. The practical consequence of these lines is that *the governing partial differential equations that describe the flow reduce to ordinary differential equations along the characteristic lines*. These equations are called the *compatibility equations,* which can be found by setting $N = 0$ in Equation (13.4), as follows. When $N = 0$, the numerator determinant yields

$$\left(1 - \frac{u^2}{a^2}\right) du\, dy + \left(1 - \frac{v^2}{a^2}\right) dx\, dv = 0$$

or

$$\frac{dv}{du} = \frac{-(1 - u^2/a^2)}{1 - v^2/a^2} \frac{dy}{dx} \tag{13.11}$$

Keep in mind that N is set to zero only when $D = 0$ in order to keep the flow-field derivatives finite, albeit of the indeterminate form $0/0$. When $D = 0$, we are restricted to considering directions *only* along the characteristic lines, as explained earlier. Hence, when $N = 0$, we are held to the same restriction. Therefore,

Equation (13.11) holds only along the characteristic lines. Therefore, in Equation (13.11),

$$\frac{dy}{dx} \equiv \left(\frac{dy}{dx}\right)_{\text{char}} \tag{13.12}$$

Substituting Equations (13.12) and (13.7) into (13.11), we obtain

$$\frac{dv}{du} = -\frac{1 - u^2/a^2}{1 - v^2/a^2} \frac{-uv/a^2 \pm \sqrt{(u^2 + v^2)/a^2 - 1}}{1 - u^2/a^2}$$

or

$$\frac{dv}{du} = \frac{uv/a^2 \mp \sqrt{(u^2 + v^2)/a^2 - 1}}{1 - v^2/a^2} \tag{13.13}$$

Recall from Figure 13.3 that $u = V\cos\theta$ and $v = V\sin\theta$. Also, $(u^2 + v^2)/a^2 = V^2/a^2 = M^2$. Hence, Equation (13.13) becomes

$$\frac{d(V\sin\theta)}{d(V\cos\theta)} = \frac{M^2\cos\theta\sin\theta \mp \sqrt{M^2 - 1}}{1 - M^2\sin^2\theta}$$

which, after some algebraic manipulations, reduces to

$$\boxed{d\theta = \mp\sqrt{M^2 - 1}\,\frac{dV}{V}} \tag{13.14}$$

Examine Equation (13.14). It is an *ordinary differential equation* obtained from the original governing partial differential equation, Equation (13.1). However, Equation (13.14) contains the restriction given by Equation (13.12); that is, Equation (13.14) holds *only* along the characteristic lines. Hence, Equation (13.14) gives the *compatibility relations* along the characteristic lines. In particular, comparing Equation (13.14) with Equation (13.10), we see that

$$d\theta = -\sqrt{M^2 - 1}\,\frac{dV}{V} \qquad \text{(applies along the } C_- \text{ characteristic)} \tag{13.15}$$

$$d\theta = \sqrt{M^2 - 1}\,\frac{dV}{V} \qquad \text{(applies along the } C_+ \text{ characteristic)} \tag{13.16}$$

Examine Equation (13.14) further. It should look familiar; indeed, Equation (13.14) is identical to the expression obtained for Prandtl-Meyer flow in Section 9.6, namely, Equation (9.32). Hence, Equation (13.14) can be integrated to obtain a result in terms of the Prandtl-Meyer function, given by Equation (9.42). In particular, the integration of Equations (13.15) and (13.16) yields

$$\theta + \nu(M) = \text{const} = K_- \qquad \text{(along the } C_- \text{ characteristic)} \tag{13.17}$$

$$\theta - \nu(M) = \text{const} = K_+ \qquad \text{(along the } C_+ \text{ characteristic)} \tag{13.18}$$

In Equation (13.17), K_- is a constant along a given C_- characteristic; it has different values for different C_- characteristics. In Equation (13.18), K_+ is a constant along a given C_+ characteristic; it has different values for different C_+ characteristics. Note that our compatibility relations are now given by Equations (13.17) and (13.18), which are *algebraic* equations which hold only along the characteristic

lines. In a general inviscid, supersonic, steady flow, the compatibility equations are ordinary differential equations; only in the case of two-dimensional irrotational flow do they further reduce to algebraic equations.

What is the advantage of the characteristic lines and their associated compatibility equations discussed above? Simply this—to solve the nonlinear supersonic flow, we need to deal only with ordinary differential equations (or in the present case, algebraic equations) instead of the original partial differential equations. Finding the solution of such ordinary differential equations is usually much simpler than dealing with partial differential equations.

How do we use the above results to solve a practical problem? The purpose of the next section is to give such an example, namely, the calculation of the supersonic flow inside a nozzle and the determination of a proper wall contour so that shock waves do not appear inside the nozzle. To carry out this calculation, we deal with two types of grid points: (1) internal points, away from the wall, and (2) wall points. Characteristics calculations at these two sets of points are carried out as follows.

13.2.1 Internal Points

Consider the internal grid points 1, 2, and 3 as shown in Figure 13.5. Assume that we know the location of points 1 and 2, as well as the flow properties at these points. Define point 3 as the intersection of the C_- characteristic through point 1 and the C_+ characteristic through point 2. From our previous discussion, $(K_-)_1 = (K_-)_3$ because K_- is constant along a given C_- characteristic. The value of $(K_-)_1 = (K_-)_3$ is obtained from Equation (13.17) evaluated at point 1:

$$(K_-)_3 = (K_-)_1 = \theta_1 + \nu_1 \tag{13.19}$$

Similarly, $(K_+)_2 = (K_+)_3$ because K_+ is constant along a given C_+ characteristic. The value of $(K_+)_2 = (K_+)_3$ is obtained from Equation (13.18) evaluated at point 2:

$$(K_+)_3 = (K_+)_2 = \theta_2 - \nu_2 \tag{13.20}$$

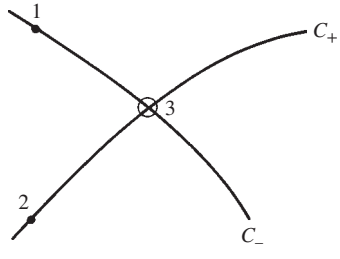

Figure 13.5 Characteristic mesh used for the location of point 3 and the calculation of flow conditions at point 3, knowing the locations and flow properties at points 1 and 2.

Now evaluate Equations (13.17) and (13.18) at point 3:

$$\theta_3 + \nu_3 = (K_-)_3 \tag{13.21}$$

and

$$\theta_3 - \nu_3 = (K_+)_3 \tag{13.22}$$

In Equations (13.21) and (13.22), $(K_-)_3$ and $(K_+)_3$ are known values, obtained from Equations (13.19) and (13.20). Hence, Equations (13.21) and (13.22) are two algebraic equations for the two unknowns θ_3 and ν_3. Solving these equations, we obtain

$$\theta_3 = \tfrac{1}{2}[(K_-)_1 + (K_+)_2] \tag{13.23}$$

$$\nu_3 = \tfrac{1}{2}[(K_-)_1 - (K_+)_2] \tag{13.24}$$

Knowing θ_3 and ν_3, all other flow properties at point 3 can be obtained as follows:

1. From ν_3, obtain the associated M_3 from Appendix C.
2. From M_3 and the known p_0 and T_0 for the flow (recall that for inviscid, adiabatic flow, the total pressure and total temperature are constants throughout the flow), find p_3 and T_3 from Appendix A.
3. Knowing T_3, compute $a_3 = \sqrt{\gamma R T_3}$. In turn, $V_3 = M_3 a_3$.

As stated earlier, point 3 is located by the intersection of the C_- and C_+ characteristics through points 1 and 2, respectively. These characteristics are curved lines; however, for purposes of calculation, we assume that the characteristics are straight-line segments between points 1 and 3 and between points 2 and 3. For example, the slope of the C_- characteristic between points 1 and 3 is assumed to be the average value between these two points, that is, $\frac{1}{2}(\theta_1 + \theta_3) - \frac{1}{2}(\mu_1 + \mu_3)$. Similarly, the slope of the C_+ characteristic between points 2 and 3 is approximated by $\frac{1}{2}(\theta_2 + \theta_3) + \frac{1}{2}(\mu_2 + \mu_3)$.

13.2.2 Wall Points

In Figure 13.6, point 4 is an internal flow point near a wall. Assume that we know all the flow properties at point 4. The C_- characteristic through point 4 intersects the wall at point 5. At point 5, the slope of the wall θ_5 is known. The flow properties at the wall point, point 5, can be obtained from the known properties at point 4 as follows. Along the C_- characteristic, K_- is constant. Hence, $(K_-)_4 = (K_-)_5$.

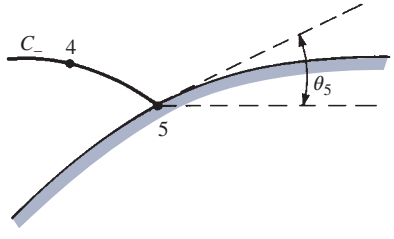

Figure 13.6 Wall point.

Moreover, the value of K_- is known from Equation (13.17) evaluated at point 4:

$$(K_-)_4 = (K_-)_5 = \theta_4 + \nu_4 \tag{13.25}$$

Evaluating Equation (13.17) at point 5, we have

$$(K_-)_5 = \theta_5 + \nu_5 \tag{13.26}$$

In Equation (13.26), $(K_-)_5$ and θ_5 are known; thus ν_5 follows directly. In turn, all other flow variables at point 5 can be obtained from ν_5 as explained earlier. The characteristic line between points 4 and 5 is assumed to be a straight-line segment with average slope given by $\frac{1}{2}(\theta_4 + \theta_5) - \frac{1}{2}(\mu_4 + \mu_5)$.

From the above discussion of both internal and wall points, we see that properties at the grid points are calculated from *known* properties at other grid points. Hence, in order to *start* a calculation using the method of characteristics, we have to know the flow properties along some *initial data* line. Then we piece together the characteristics mesh and associated flow properties by "marching downstream" from the initial data line. This is illustrated in the next section.

We emphasize again that the method of characteristics is an exact solution of inviscid, nonlinear supersonic flow. However, in practice, there are numerical errors associated with the finite grid; the approximation of the characteristics mesh by straight-line segments between grid points is one such example. In principle, the method of characteristics is truly exact only in the limit of an infinite number of characteristic lines.

We have discussed the method of characteristics for two-dimensional, irrotational, steady flow. The method of characteristics can also be used for rotational and three-dimensional flows, as well as unsteady flows. See Reference 21 for more details.

13.3 SUPERSONIC NOZZLE DESIGN

In Chapter 10, we demonstrated that a nozzle designed to expand a gas from rest to supersonic speeds must have a convergent-divergent shape. Moreover, the quasi-one-dimensional analysis of Chapter 10 led to the prediction of flow properties as a function of x through a nozzle of specified shape (see, e.g., Figure 10.10). The flow properties at any x station obtained from the quasi-one-dimensional analysis represent an *average* of the flow over the given nozzle cross section. The beauty of the quasi-one-dimensional approach is its simplicity. On the other hand, its disadvantages are (1) it cannot predict the details of the actual three-dimensional flow in a convergent-divergent nozzle and (2) it gives no information on the proper wall contour of such nozzles.

The purpose of the present section is to describe how the method of characteristics can supply the above information which is missing from a quasi-one-dimensional analysis. For simplicity, we treat a two-dimensional flow, as sketched in Figure 13.7. Here, the flow properties are a function of x and y. Such a two-dimensional flow is applicable to supersonic nozzles of rectangular cross section, such as sketched in the insert at the top of Figure 13.7. Two-dimensional

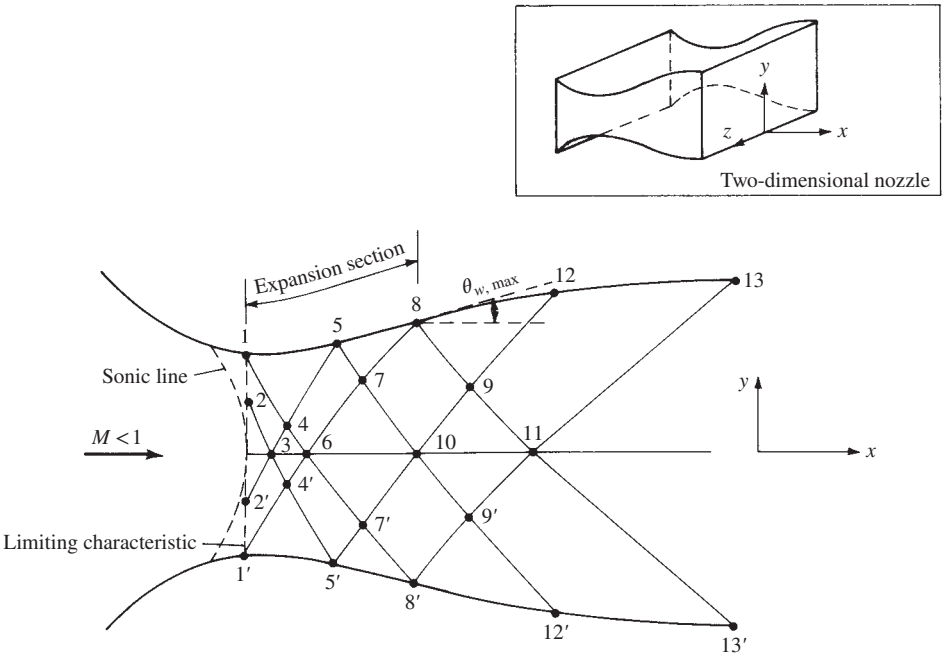

Figure 13.7 Schematic of supersonic nozzle design by the method of characteristics.

(rectangular) nozzles are used in many supersonic wind tunnels. They are also the heart of gas-dynamic lasers (see Reference 1). In addition, there is current discussion of employing rectangular exhaust nozzles on advanced military jet airplanes envisaged for the future.

Consider the following problem. We wish to design a convergent-divergent nozzle to expand a gas from rest to a given supersonic Mach number at the exit M_e. How do we design the proper contour so that we have shock-free, isentropic flow in the nozzle? The answer to this question is discussed in the remainder of this section.

For the convergent, subsonic section, there is no specific contour which is better than any other. There are rules of thumb based on experience and guided by subsonic flow theory; however, we are not concerned with the details here. We simply assume that we have a reasonable contour for the subsonic section.

Due to the two-dimensional nature of the flow in the throat region, the sonic line is generally curved, as sketched in Figure 13.7. A line called the *limiting characteristic* is sketched just downstream of the sonic line. The limiting characteristic is defined such that any characteristic line originating downstream of the limiting characteristic does not intersect the sonic line; in contrast, a characteristic line originating in the small region between the sonic line and the limiting characteristic can intersect the sonic line (for more details on the limiting characteristic, see Reference 21). To begin a method of characteristics solution, we must use an initial data line which is downstream of the limiting characteristic.

Let us assume that by independent calculation of the subsonic-transonic flow in the throat region, we know the flow properties at all points on the limiting characteristic. That is, we use the limiting characteristic as our initial data line. For example, we know the flow properties at points 1 and 2 on the limiting characteristic in Figure 13.7. Moreover, consider the nozzle contour just downstream of the throat. Letting θ denote the angle between a tangent to the wall and the horizontal, the section of the divergent nozzle where θ is increasing is called the *expansion section,* as shown in Figure 13.7. The end of the expansion section occurs where $\theta = \theta_{max}$ (point 8 in Figure 13.7). Downstream of this point, θ decreases until it equals zero at the nozzle exit. The portion of the contour where θ decreases is called the *straightening section*. The shape of the expansion section is somewhat arbitrary; typically, a circular arc of large radius is used for the expansion section of many wind-tunnel nozzles. Consequently, in addition to knowing the flow properties along the limiting characteristic, we also have an expansion section of specified shape; that is, we know θ_1, θ_5, and θ_8 in Figure 13.7. The purpose of our application of the method of characteristics now becomes the proper design of the contour of the straightening section (from points 8 to 13 in Figure 13.7).

The characteristics mesh sketched in Figure 13.7 is very coarse—this is done intentionally to keep our discussion simple. In an actual calculation, the mesh should be much finer. The characteristics mesh and the flow properties at the associated grid points are calculated as follows:

1. Draw a C_- characteristic from point 2, intersecting the centerline at point 3. Evaluating Equation (13.17) at point 3, we have

$$\theta_3 + \nu_3 = (K_-)_3$$

In the above equation, $\theta_3 = 0$ (the flow is horizontal along the centerline). Also, $(K_-)_3$ is known because $(K_-)_3 = (K_-)_2$. Hence, the above equation can be solved for ν_3.

2. Point 4 is located by the intersection of the C_- characteristic from point 1 and the C_+ characteristic from point 3. In turn, the flow properties at the internal point 4 are determined as discussed in the last part of Section 13.2.

3. Point 5 is located by the intersection of the C_+ characteristic from point 4 with the wall. Since θ_5 is known, the flow properties at point 5 are determined as discussed in Section 13.2 for wall points.

4. Points 6 through 11 are located in a manner similar to the above, and the flow properties at these points are determined as discussed before, using the internal point or wall point method as appropriate.

5. Point 12 is a wall point on the straightening section of the contour. The purpose of the straightening section is to cancel the expansion waves generated by the expansion section. Hence, there are no waves which are reflected from the straightening section. In turn, no right-running waves cross the characteristic line between points 9 and 12. As a result, the

characteristic line between points 9 and 12 is a straight line, along which θ is constant, that is, $\theta_{12} = \theta_9$. The section of the wall contour between points 8 and 12 is approximated by a straight line with an average slope of $\frac{1}{2}(\theta_8 + \theta_{12})$.

6. Along the centerline, the Mach number continuously increases. Let us assume that at point 11, the design exit Mach number M_e is reached. The characteristic line from points 11 to 13 is the last line of the calculation. Again, $\theta_{13} = \theta_{11}$, and the contour from point 12 to point 13 is approximated by a straight-line segment with an average slope of $\frac{1}{2}(\theta_{12} + \theta_{13})$.

The above description is intended to give you a "feel" for the application of the method of characteristics. If you wish to carry out an actual nozzle design, and/or if you are interested in more details, read the more complete treatments in References 21 and 32.

Note in Figure 13.7 that the nozzle flow is symmetrical about the centerline. Hence, the points below the centerline (1′, 2′, 3′, etc.) are simply mirror images of the corresponding points above the centerline. In making a calculation of the flow through the nozzle, we need to concern ourselves only with those points in the upper half of Figure 13.7, above and on the centerline.

13.4 ELEMENTS OF FINITE-DIFFERENCE METHODS

The method of characteristics described in the previous section legitimately can be considered a part of computational fluid dynamics because it uses discrete algebraic forms of the governing equations [such as Equations (13.17) and (13.18)] which are solved at discrete points in the flow (the characteristic mesh illustrated in Figure 13.5). However, most authors consider that CFD is represented by mainly finite difference and finite volume techniques, such as are discussed in Reference 60, and the method of characteristics is usually not included in the study of CFD. The purpose of this section is to give you the flavor of finite-difference techniques by describing one particular method that is readily applicable to a number of compressible flow problems. The method discussed here is representative of mainstream CFD, but it is just the tip of the iceberg of CFD. The intensive research in CFD since 1960 has produced a multitude of different algorithms and philosophies, and it is far beyond the scope of this book to go into the details of such work. See Reference 60 for an in-depth presentation of CFD at the introductory level. In addition, you are strongly encouraged to read the current literature in this regard, in particular the *AIAA Journal, Computers and Fluids,* and the *Journal of Computational Physics*. Finally, in this chapter we are dealing with numerical solutions of *inviscid supersonic* flows. See Reference 21 for an expanded discussion of finite difference methods applied to supersonic flows.

First, recall the discrete finite difference representations for partial derivatives that were derived in Section 2.17.2 using Taylors series. In particular, we recall

Equations (2.168), (2.171), and (2.174), repeated and renumbered, respectively, below for convenience:

$$\left(\frac{\partial u}{\partial x}\right)_{i,j} = \frac{u_{i+1,j} - u_{i,j}}{\Delta x} \qquad \text{(forward difference)} \qquad (13.27)$$

$$\left(\frac{\partial u}{\partial x}\right)_{i,j} = \frac{u_{i,j} - u_{i-1,j}}{\Delta x} \qquad \text{(rearward difference)} \qquad (13.28)$$

$$\left(\frac{\partial u}{\partial x}\right)_{i,j} = \frac{u_{i+1,j} - u_{i-1,j}}{2\Delta x} \qquad \text{(central difference)} \qquad (13.29)$$

Analogous expressions for the derivatives in the y direction are as follows:

$$\left(\frac{\partial u}{\partial y}\right)_{i,j} = \begin{cases} \dfrac{u_{i,j+1} - u_{i,j}}{\Delta y} & \text{(forward difference)} \\ \dfrac{u_{i,j} - u_{i,j-1}}{\Delta y} & \text{(rearward difference)} \\ \dfrac{u_{i,j+1} - u_{i,j-1}}{2\Delta y} & \text{(central difference)} \end{cases}$$

How do we use the finite differences obtained here? Imagine that a flow in xy space is covered by the mesh shown in Figure 13.2*b*. Assume there are N grid points. At each one of these grid points, evaluate the continuity, momentum, and energy equations with their partial derivatives replaced by the finite-difference expressions derived above. For example, replacing the derivatives in Equations (7.40), (7.42*a* and *b*), and (7.44) with finite differences, along with Equations (7.1) and (7.6*a*), we obtain a system (over all N grid points) of $6N$ simultaneous nonlinear algebraic equations in terms of the $6N$ unknowns, namely, ρ, u, v, p, T, and e, at each of the N grid points. In principle, we could solve this system for the unknown flow variables at all the grid points. In practice, this is easier said than done. There are severe problems in solving such a large number of simultaneous nonlinear equations. Moreover, we have to deal with problems associated with numerical instabilities that sometimes cause such attempted solutions to "blow up" on the computer. Finally, and most importantly, we must properly account for the boundary conditions. These considerations make all finite-difference solutions a nontrivial endeavor. As a result, a number of specialized finite-difference techniques have evolved, directed at solving different types of flow problems and attempting to increase computational efficiency and accuracy. It is beyond the scope of this book to describe these difference techniques in detail. However, one technique in particular was widely used during the 1970s and 1980s. This is an approach developed in 1969 by Robert MacCormack at the NASA Ames Research Center. Because of its widespread use and acceptance at the time, as well as its relative simplicity, we will describe MacCormack's technique in enough detail to give you a reasonable understanding of the method. This description will be carried out in the context of the following example.

Consider the two-dimensional supersonic flow through the divergent duct shown in Figure 13.8*a*. Assume the flow is supersonic at the inlet, and that all

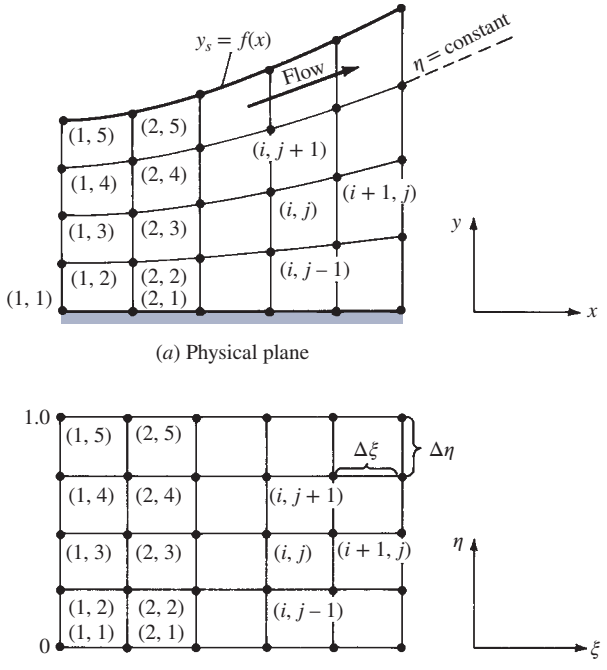

Figure 13.8 Finite-difference meshes in both the physical and computational planes.

properties are known at the inlet. That is, the flow-field variables at grid points (1, 1), (1, 2), (1, 3), (1, 4), and (1, 5) are known. The duct is formed by a flat surface at the bottom and a specified contour, $y_s = f(x)$, at the top. In addition, assume that the flow is inviscid, adiabatic, and steady, and with no body forces. It can be rotational or irrotational—the method of solution is the same. The governing equations are obtained from Equations (7.40), (7.42*a* and *b*), (7.44), (7.1), and (7.6*a*), which yield

$$\frac{\partial(\rho u)}{\partial x} + \frac{\partial(\rho v)}{\partial y} = 0 \tag{13.30}$$

$$\rho u \frac{\partial u}{\partial x} + \rho v \frac{\partial u}{\partial y} = -\frac{\partial p}{\partial x} \tag{13.31}$$

$$\rho u \frac{\partial v}{\partial x} + \rho v \frac{\partial v}{\partial y} = -\frac{\partial p}{\partial y} \tag{13.32}$$

$$\rho u \frac{\partial(e + V^2/2)}{\partial x} + \rho v \frac{\partial(e + V^2/2)}{\partial y} = -\frac{\partial(pu)}{\partial x} - \frac{\partial(pv)}{\partial y} \tag{13.33}$$

$$p = \rho RT \tag{13.34}$$

$$e = c_v T \tag{13.35}$$

Let us express these equations in slightly different form, as follows. Multiplying Equation (13.30) by u, and adding the results to Equation (13.31), we have

$$u\frac{\partial(\rho u)}{\partial x} + \rho u\frac{\partial u}{\partial x} + u\frac{\partial(\rho v)}{\partial y} + \rho v\frac{\partial u}{\partial y} = -\frac{\partial p}{\partial x}$$

or

$$\frac{\partial(\rho u^2)}{\partial x} + \frac{\partial(\rho uv)}{\partial y} = -\frac{\partial p}{\partial x}$$

or

$$\frac{\partial}{\partial x}(\rho u^2 + p) = -\frac{\partial(\rho uv)}{\partial y} \tag{13.36}$$

Similarly, multiplying Equation (13.30) by v, and adding the result to Equation (13.32), we obtain

$$\frac{\partial(\rho uv)}{\partial x} = -\frac{\partial(\rho v^2 + p)}{\partial y} \tag{13.37}$$

Multiplying Equation (13.30) by $e + V^2/2$, and adding the result to Equation (13.33), we obtain

$$\frac{\partial}{\partial x}\left[\rho u\left(e + \frac{V^2}{2}\right) + pu\right] = -\frac{\partial}{\partial y}\left[\rho v\left(e + \frac{V^2}{2}\right) + pv\right] \tag{13.38}$$

Define the following symbols:

$$F = \rho u \tag{13.39a}$$

$$G = \rho u^2 + p \tag{13.39b}$$

$$H = \rho uv \tag{13.39c}$$

$$K = \rho u\left(e + \frac{V^2}{2}\right) + pu \tag{13.39d}$$

Then, Equations (13.30) and (13.36) to (13.38) become

$$\frac{\partial F}{\partial x} = -\frac{\partial(\rho v)}{\partial y} \tag{13.40}$$

$$\frac{\partial G}{\partial x} = -\frac{\partial(\rho uv)}{\partial y} \tag{13.41}$$

$$\frac{\partial H}{\partial x} = -\frac{\partial(\rho v^2 + p)}{\partial y} \tag{13.42}$$

$$\frac{\partial K}{\partial x} = -\frac{\partial}{\partial y}\left[\rho v\left(e + \frac{V^2}{2}\right) + pv\right] \tag{13.43}$$

Equations (13.40) to (13.43) are the continuity, x and y momentum, and energy equations, respectively—but in a slightly different form from those we are used

to seeing. The above form of these equations is frequently called the *conservation form*. Let us now treat F, G, H, and K as our primary dependent variables; these quantities are called *flux variables,* in contrast to the usual p, ρ, T, u, v, e, etc., which are called *primitive variables*. It is important to note that once the values of F, G, H, and K are known at a given grid point, the primitive variables at that point can be found from Equations (13.39*a* to *d*) and

$$p = \rho RT \tag{13.44}$$

$$e = c_v T \tag{13.45}$$

$$V^2 = u^2 + v^2 \tag{13.46}$$

That is, Equations (13.39*a* to *d*) and (13.44) to (13.46) constitute seven algebraic equations for the seven primitive variables, ρ, u, v, p, e, T, and V.

Let us return to the physical problem given in Figure 13.8*a*. Because the duct diverges, it is difficult to deal with an orthogonal, rectangular mesh; rather, a mesh which conforms to the boundary of the system will be curved, as shown in Figure 13.8*a*. On the other hand, to use our finite-difference quotients as given in Equation (13.27), (13.28), or (13.29), we desire a rectangular computational mesh. Therefore, we must *transform* the curved mesh shown in Figure 13.8*a*, known as the *physical plane,* to a rectangular mesh shown in Figure 13.8*b*, known as the *computational plane*. This transformation can be carried out as follows. Define

$$\xi = x \tag{13.47a}$$

$$\eta = \frac{y}{y_s}$$

where

$$y_s = f(x) \tag{13.47b}$$

In the above transformation, η ranges from 0 at the bottom wall to 1.0 at the top wall. In the computational plane (Figure 13.8*b*), η = constant is a straight horizontal line, whereas in the physical plane, η = constant corresponds to the curved line shown in Figure 13.8. Because we wish to apply our finite differences in the computational plane, we need the governing equations in terms of ξ and η rather than x and y. To accomplish this transformation, apply the chain rule of differentiation, using Equation (13.47*a* and *b*) as follows:

$$\frac{\partial}{\partial x} = \frac{\partial}{\partial \xi}\frac{\partial \xi}{\partial x} + \frac{\partial}{\partial \eta}\frac{\partial \eta}{\partial x} = \frac{\partial}{\partial \xi} - \frac{y}{y_s^2}\frac{dy_s}{dx}\frac{\partial}{\partial \eta}$$

or

$$\frac{\partial}{\partial x} = \frac{\partial}{\partial \xi} - \left(\frac{\eta}{y_s}\frac{dy_s}{dx}\right)\frac{\partial}{\partial \eta} \tag{13.48}$$

and

$$\frac{\partial}{\partial y} = \frac{\partial}{\partial \xi}\frac{\partial \xi}{\partial y} + \frac{\partial}{\partial \eta}\frac{\partial \eta}{\partial y} = \frac{1}{y_s}\frac{\partial}{\partial \eta} \tag{13.49}$$

Using Equations (13.48) and (13.49), we see that Equations (13.40) to (13.43) become

$$\frac{\partial F}{\partial \xi} = \left(\frac{\eta}{y_s}\frac{dy_s}{dx}\right)\left(\frac{\partial F}{\partial \eta}\right) - \frac{1}{y_s}\frac{\partial(\rho v)}{\partial \eta} \tag{13.50}$$

$$\frac{\partial G}{\partial \xi} = \left(\frac{\eta}{y_s}\frac{dy_s}{dx}\right)\frac{\partial G}{\partial \eta} - \frac{1}{y_s}\frac{\partial(\rho u v)}{\partial \eta} \tag{13.51}$$

$$\frac{\partial H}{\partial \xi} = \left(\frac{\eta}{y_s}\frac{dy_s}{dx}\right)\frac{\partial H}{\partial \eta} - \frac{1}{y_s}\frac{\partial(\rho v^2 + p)}{\partial \eta} \tag{13.52}$$

$$\frac{\partial K}{\partial \xi} = \left(\frac{\eta}{y_s}\frac{dy_s}{dx}\right)\frac{\partial K}{\partial \eta} - \frac{1}{y_s}\frac{\partial}{\partial \eta}\left[\rho v\left(e + \frac{V^2}{2}\right) + pv\right] \tag{13.53}$$

Note in the above equations that the ξ derivatives are on the left and the η derivatives are all grouped on the right.

Let us now concentrate on obtaining a numerical, finite-difference solution of the problem shown in Figure 13.8. We will deal exclusively with the computational plane, Figure 13.8*b*, where the governing continuity, x and y momentum, and energy equations are given by Equations (13.50) to (13.53), respectively. Grid points (1, 1), (2, 1), (1, 2), (2, 2), etc., in the computational plane are the same as grid points (1, 1), (2, 1), (1, 2), (2, 2), etc., in the physical plane. All the flow variables are known at the inlet, including F, G, H, and K. The solution for the flow variables downstream of the inlet can be found by using MacCormack's method, which is based on Taylor's series expansions for F, G, H, and K as follows:

$$F_{i+1,j} = F_{i,j} + \left(\frac{\partial F}{\partial \xi}\right)_{\text{ave}} \Delta\xi \tag{13.54a}$$

$$G_{i+1,j} = G_{i,j} + \left(\frac{\partial G}{\partial \xi}\right)_{\text{ave}} \Delta\xi \tag{13.54b}$$

$$H_{i+1,j} = H_{i,j} + \left(\frac{\partial H}{\partial \xi}\right)_{\text{ave}} \Delta\xi \tag{13.54c}$$

$$K_{i+1,j} = K_{i,j} + \left(\frac{\partial K}{\partial \xi}\right)_{\text{ave}} \Delta\xi \tag{13.54d}$$

In Equation (13.54*a* to *d*), F, G, H, and K at point (i,j) are considered known, and these equations are used to find F, G, H, and K at point $(i+1,j)$ assuming that we can calculate the values of $(\partial F/\partial \xi)_{\text{ave}}$, $(\partial G/\partial \xi)_{\text{ave}}$, etc. The main thrust of MacCormack's method is the calculation of these average derivatives. Examining Equation (13.54*a* to *d*), we find that this finite-difference method is clearly a "down-stream marching" method; given the flow at point (i,j) we use Equation (13.54*a* to *d*) to find the flow at point $(i+1,j)$. Then the process is repeated to find the flow at point $(i+2,j)$, etc. This downstream marching is similar to that performed with the method of characteristics.

The average derivatives in Equation (13.54*a* to *d*) are found by means of a straightforward "predictor-corrector" approach, outlined below. In carrying out this approach, we assume that the flow properties are known at grid point (i,j), as well as at all points directly above and below (i,j), namely, at $(i,j+1)$, $(i,j+2)$, $(i,j-1)$, $(i,j-2)$, etc.

13.4.1 Predictor Step

First, predict the value of $F_{i+1,j}$ by using a Taylor series where $\partial F/\partial\xi$ is evaluated at point (i,j). Denote this predicted value by $\bar{F}_{i+1,j}$:

$$\bar{F}_{i+1,j} = F_{i,j} + \left(\frac{\partial F}{\partial \xi}\right)_{i,j} \Delta\xi \tag{13.55}$$

In Equation (13.55), $(\partial F/\partial\xi)_{i,j}$ is obtained from the continuity equation, Equation (13.50), using *forward differences* for the η derivatives; that is,

$$\left(\frac{\partial F}{\partial \xi}\right)_{i,j} = \left(\frac{\eta}{y_s}\frac{dy_s}{dx}\right)_{i,j}\left(\frac{F_{i,j+1}-F_{i,j}}{\Delta\eta}\right) - \frac{1}{y_s}\left[\frac{(\rho v)_{i,j+1}-(\rho v)_{i,j}}{\Delta\eta}\right] \tag{13.56}$$

In Equation (13.56), all quantities on the right-hand side are known and allow the calculation of $(\partial F/\partial\xi)_{i,j}$ which is, in turn, inserted into Equation (13.55). A similar procedure is used to find predicted values of G, H, and K, namely, $\bar{G}_{i+1,j}$, $\bar{H}_{i+1,j}$, and $\bar{K}_{i+1,j}$, using forward differences in Equations (13.51) to (13.53). In turn, predicted values of the primitive variables, $\bar{p}_{i+1,j}$, $\bar{\rho}_{i+1,j}$, etc., can be obtained from Equations (13.39*a* to *d*) and (13.44) to (13.46).

13.4.2 Corrector Step

The predicted values obtained above are used to obtain predicted values of the derivative $(\overline{\partial F/\partial\xi})_{i+1,j}$, using *rearward differences* in Equation (13.50):

$$\left(\frac{\overline{\partial F}}{\partial \xi}\right)_{i+1,j} = \left(\frac{\eta}{y_s}\frac{dy_s}{dx}\right)_{i+1,j}\frac{\bar{F}_{i+1,j}-\bar{F}_{i+1,j-1}}{\Delta\eta} - \frac{1}{y_s}\frac{(\overline{\rho v})_{i+1,j}-(\overline{\rho v})_{i+1,j-1}}{\Delta\eta} \tag{13.57}$$

In turn, the results from Equations (13.56) and (13.57) allow the calculation of the average derivative

$$\left(\frac{\partial F}{\partial \xi}\right)_{\text{ave}} = \frac{1}{2}\left[\left(\frac{\partial F}{\partial \xi}\right)_{i,j} + \left(\frac{\overline{\partial F}}{\partial \xi}\right)_{i+1,j}\right] \tag{13.58}$$

Finally, this average derivative is used in Equation (13.54*a*) to obtain the corrected value of $F_{i+1,j}$. The same process is followed to find the corrected values of $G_{i+1,j}$, $H_{i+1,j}$, and $K_{i+1,j}$ using rearward differences in Equations (13.51) to (13.53) and calculating the average derivatives $(\partial G/\partial\xi)_{\text{ave}}$, etc., in the same manner as Equation (13.58).

The above finite-difference procedure allows the step-by-step calculation of the flow field, marching downstream from some initial data line. In the flow given

in Figure 13.8, the initial data line is the inlet, where properties are considered known. Although all the calculations are carried out in the transformed, computational plane, the flow-field results obtained at points (2, 1), (2, 2), etc., in the computational plane are the same values at points (2, 1), (2, 2), etc., in the physical plane.

There are other aspects of the finite-difference solution which have not been described above. For example, what values of $\Delta\eta$ and $\Delta\xi$ in Equations (13.54*a* to *d*), (13.55), (13.56), and (13.57) are allowed in order to maintain numerical stability? How is the flow-tangency condition at the walls imposed on the finite-difference calculations? These are important matters, but we do not take the additional space to discuss them here. See Chapter 11 of Reference 21 for details on these questions. Our purpose here has been to give you only a feeling for the nature of the finite-difference method.

13.5 THE TIME-DEPENDENT TECHNIQUE: APPLICATION TO SUPERSONIC BLUNT BODIES

The method of characteristics described in Section 13.2 is applicable only to supersonic flows; the characteristic lines are not defined in a practical fashion for steady, subsonic flow. Also, the particular finite-difference method outlined in Section 13.4 applies only to supersonic flows; if it were to be used in a locally subsonic region, the calculation would blow up. The reason for both of the above comments is that the method of characteristics and the steady flow, forward-marching finite-difference technique depend on the governing equations being mathematically "hyperbolic." In contrast, the equations for steady subsonic flow are "elliptic." (See Reference 21 for a description of these mathematical classifications.) The fact that the governing equations change their mathematical nature in going from locally supersonic to locally subsonic flow has historically caused theoretical aerodynamicists much grief. One problem in particular, namely, the mixed subsonic-supersonic flow over a supersonic blunt body as described in Section 9.5, was a major research area until a breakthrough was made in the late 1960s for its proper numerical solution. The purpose of this section is to describe a numerical finite-difference solution which readily allows the calculation of mixed subsonic-supersonic flows—the *time-dependent method*—and to show how it is used to solve supersonic blunt-body flows. Time-dependent techniques are very common in modern computational fluid dynamics, and as a student of aerodynamics, you should be familiar with their philosophy. These techniques are also called *time-marching techniques* because the solutions are obtained by marching in steps of time.

Consider a blunt body in a supersonic stream, as sketched in Figure 13.9*a*. The shape of the body is known and is given by $b = b(y)$. For a given freestream Mach number M_∞, we wish to calculate the shape and location of the detached shock wave, as well as the flow-field properties between the shock and the body.